Physics of the Solid State, 2023, Vol. 65, No. 10

03,13

Physical and optical properties of polycrystalline $Cu_{0.27}Ga_{1.85}Se_{1.88}$ and $Cu_{0.33}Ga_{1.54}Se_{2.13}$, films synthesized by controlled selenization

© O.B. Romanova[1], Yu.V. Gerasimova[1,2], T.M. Gadzhiev[3], S.S. Aplesnin[1,4], A.S. Aleksandrovsky[1,2], M.N. Sitnikov[4], M.A. Aliev[3], L.V. Udod[1,4], H. Abdelbaki[4]

[1] Kirensky Institute of Physics, Federal Research Center KSC SB, Russian Academy of Sciences, Krasnoyarsk, Russia
[2] Institute of Engineering Physics and Radioelectronics, Siberian Federal University, Krasnoyarsk, Russia
[3] Amirkhanov Institute of Physics, Dagestan Federal Research Center, Russian Academy of Sciences, Makhachkala, Russia
[4] Siberian State University of Science and Technology, Krasnoyarsk, Russia

E-mail: rob@iph.krasn.ru

Received May 25, 2023
Revised July 18, 2023
Accepted September 4, 2023

Polycrystalline films of $Cu_{0.27}Ga_{1.85}Se_{1.88}$ and $Cu_{0.33}Ga_{1.54}Se_{2.13}$ with a chalcopyrite structure of the Cu−Ga−Se system were synthesized. The effect of selenization temperature on the chemical composition and structure of films was studied by X-ray phase analysis and electron microscopy. The dependence of film resistance on concentration and temperature has been studied. The effect of photoconductivity was discovered on $Cu_{0.27}Ga_{1.85}Se_{1.88}$ films. The Raman spectra of these films were calculated. From the absorption spectra, the Urbach energy $E_U = 0.9$ eV was determined, which indicates a nouniform distribution of localized states in the electronic structure of the films. Migration and dipole-orientation contributions to the electrical polarization of the films have been established. Using the Debye model, the relaxation time in film samples of the Cu−Ga−Se system was calculated.

Keywords: polycrystalline films, synthesis of films of the Cu−Ga−Se system, Raman spectra, electrical properties, photoconductivity.

DOI: 10.61011/PSS.2023.10.57213.90

1. Introduction

Semiconductor compounds of type (I-III-VI_2) [1–4] are promising for use in photonics and optoelectronics. These ternary compounds crystallize in the chalcopyrite structure. Materials based on $Cu(In_{1-x},Ga_x)Se_2$ or (CIGS) solid solutions are also promising for use in thin-film solar cells. CIGS solar cells achieve up to 21.7% efficiency, exhibit increased short circuit current density (JSC), high open circuit voltage (UOC) and improved fill factors (FF)[5–7]. These compositions are not inferior in quality to single-junction materials of GaAs solar cells on a substrate [8]. By changing the CIGS composition you can adjust its properties, in particular, the band gap E_g from 1.01 to 1.48 eV. Such a smooth change E_g of CIGS solid solutions [9] corresponds to the infrared and visible regions of the electromagnetic radiation spectrum, as for GaAs-based materials [10]. In this regard, obtaining and studying the physical effects of new compositions of film materials based on Cu−Ga−Se are important tasks for modifying solar cells.

By changing the concentration of Cu/Ga components in the Cu−Ga−Se system, you can monotonically change the band gap of the compound $CuGaSe_2$ [11]. Thus, in the synthesized thin-film compounds, the band gap increased from 1.68 eV for $CuGaSe_2$, where Cu/Ga = 0.85 to 1.85 eV for $CuGa_3Se_5$, where Cu/Ga = 0.33. A study of the photosensitivity of these films showed that samples $CuGaSe_2$ show a photocurrent density of — 19.0 mA/cm^2. This is greater compared to films of the composition $CuGa_3Se_5$ (where Cu/Ga = 0.33), where the photocurrent density was — 12.1 mA/cm^2. The decrease in the photocurrent density of $CuGa_3Se_5$ compared to $CuGaSe_2$ is associated with increase in the band gap, as well as with increase in the density of defects and grain boundaries in $CuGa_3Se_5$. Such defects play the role of recombination centers for photoexcited charge carriers.

CuGaSe single crystals$_2$are p-type semiconductors, and they can be divided into two groups, low-resistance ($\rho = 10^2-10^4\,\Omega\cdot$cm) and high-resistance ($\rho = 10^5-10^7\,\Omega\cdot$cm) samples. Studies were carried out on the γ-irradiation effect on the conductivity of $CuGaSe_2$. It was found that the resistivity of low-resistance samples increases with increase in radiation γ-dose, and the resistance of high-resistance samples does not depend on the radiation dose [12]. Photoconductivity and luminescence were studied in the temperature range 90−300 K on $CuGaSe_2$ single-crystals [13]. The features of the photoconductivity spectra at 90 K are explained by interband transitions and transitions from the splitting levels of the valence band and the excited

3d level of copper to the top of the valence band. The luminescence spectra are affected by the near-surface layer of the single-crystal $CuGaSe_2$. The energy structure of the conduction band and excitation properties in the single-crystal $CuGaSe_2$ are considered in the paper [14]. Data obtained from the absorption spectra of a thin film $CuGaSe_2$ (CGSe), in particular, the band gap (E_g) CGSe $E_g = 1.64$ eV as a function of [Ga]/[Cu] are used in solar cell ZnO/CdS/$CuGaSe_2$ [15].

The review [16] discusses devices based on film $CuGaSe_2$ with $E_g = 1.7$ eV and solar cells. The differences observed between $CuGaSe_2$ and $CuInSe_2$ or $Cu(In, Ga)Se_2$ films and device properties are discussed, as well as correlation of properties taking into account the effects of alkali metals.

The mechanisms of electron transport of thin-film solar cells based on $CuGaSe_2$ are considered in the paper [17]. The dependences of transport mechanisms in heterojunction solar cells based on $CuGaSe_2$ on stoichiometry, type of substrate, and deposition temperature of CdS buffer layer were studied. It was established that the determining parameter of the electron loss mechanism is the doping level of the absorbing layer. Doping is affected by the type of stoichiometry deviation, as well as by the content of additional elements in the substrate, for example, such as Na, which significantly deteriorates their quality.

An important aspect in the photoconductivity effect manifestation is the method of obtaining the material, in particular, the single crystal $CuGaSe_2$ [18].

The dependence of Se beam equivalent pressure (BEP) during film growth on the density of defects in solar cells based on CIGS was studied using the admittance spectroscopy method [19]. It was notes that BEP Se $(1.3 \cdot 10^3–4.4 \cdot 10^3$ Pa) affects the deficiency of both Se, and Cu. Increase in phase $Cu(In, Ga)_3Se_5$ content was observed upon BEP Se decreasing. It was shown that occurrence of traps with activation energies of 300 meV can be associated with divacancy complex $V_{Se}-V_{Cu}$. So, beam Se pressure shall be monitored to obtain high-performance solar cells.

Films $Cu(In_xGa_{1-x})Se_2$ (CIGS), grown in different Se flows were studied by positron annihilation spectroscopy [20]. Increased defect phase of $Cu(In, Ga)_3Se_5$ was observed in films grown at lower flow of Se. The line shape parameter (S) of positron annihilation spectra was used to characterize defects in CIGS films. With the Se flow decreasing, the parameter S on the surface and in the near-surface region of the films increases. This phenomenon is associated with the increased concentration of the defects complex formed between Se and Cu vacancies.

In the paper [21] CIGS films were obtained using a three-stage growth method. This method is sensitive to critical compositions, including stoichiometric compositions with ratio Cu/In + Ga, with sufficient Se supply. The solar cell manufactured using the resulting CIGS film showed an active area conversion efficiency of 16.4% without the antireflection coating use. It is shown that segregation of excess Na damages CIGS surface, and this defect is repaired by sputtering pressure optimization of the underlaying molybdenum layer.

Physics of interfacial and bulk defects at the interface and in bulk of thin film photovoltaics based on $CuInSe_2$ were studied in the review [22]. Using electron probe micro-analyzer and synchronous X-ray diffraction method in paper [23] a Cu-dependent phase transition in thin polycrystalline films of $CuGaSe_2$ was studied. It was shown that in section $Cu_2Se-Ga_2Se_3$ the composition of the obtained films varies from stoichiometric $CuGaSe_2$ $(1:1:2)$ towards the gallium-rich side. Paper [24] shows limitations of devices capacity, role of defects and interfaces for capacity of solar cells $Cu(In, Ga)Se_2$ with heterojunction. It is shown that defects monitoring is ensured for two, maximum three stages, during film growth, during heterojunction formation, and, may be, during one stage of treatment after deposition.

The above brief review shows that producing the polycrystalline films of Cu–Ga–Se system with specified stoichiometry and study of their optical and electro-physical properties are actual to develop effective photoconverters.

This paper purpose is obtaining polycrystalline films with compositions of $Cu_{0.27}Ga_{1.85}Se_{1.88}$ and $Cu_{0.33}Ga_{1.54}Se_{2.13}$ and studying their optical, electro-physical and photoelectrical properties.

2. Synthesis of films and measurement methods

The polycrystalline films of $Cu_{0.27}Ga_{1.85}Se_{1.88}$ and $Cu_{0.33}Ga_{1.54}Se_{2.13}$ were obtained by two-stage method of controlled selenization of intermetal layers of Cu–Ga pre-deposited on glass substrates in two-zone thermal diffusion unit with participation of the carrier-gas (N_2) of reaction component Se. The selenization temperature (T_{sel}) in reaction zone of layers Cu–Ga with Se varies in the range 200°C$\leq T_{sel} \leq$ 550°C, and pressure of vapor-gas mixture Se + N_2 at the re-crystallization stage was increased from 10^{-4} to 10^{-1} Pa. Concentration of copper and gallium in Cu–Ga–Se system depended on the film selenization temperature. Samples $Cu_{0.27}Ga_{1.85}Se_{1.88}$ (*1*) $Cu_{0.33}Ga_{1.54}Se_{2.13}$ (*2*) and $Cu_{0.25}Ga_{0.58}Se$ (*3*) were obtained at $T_{sel} = 500$, 450 and 350°C, respectively [25].

X-ray phase studies were performed at X-ray diffraction meter Empyrean Series 2 (PANalytical, the Netherlands) using Cu-Kα radiation (1.5405 Å), scanning angles: 10–140°, β-filter. Phases were identified by comparison of obtained in experiment interplanar spacings d with data of card-index of Joint Committee on Powder Diffraction Standard (JCPDS).

Film morphology, quantitative and semiquantitative element analysis, as well as element mapping of surface of films $Cu_{0.27}Ga_{1.85}Se_{1.88}$ and $Cu_{0.33}Ga_{1.54}Se_{2.13}$ at different zoom were obtained by method of scanning electron microscopy S5500 (Hitachi, Japan).

Dielectric constant and dielectric losses and were determined by values of capacity and tangent of loss angle

measured at AM-3028 component analyzer in the range of frequencies 10^2-10^6 Hz and temperatures 300−500 K.

The electrophysical measurements of $Cu_{0.27}Ga_{1.85}Se_{1.88}$ and $Cu_{0.33}Ga_{1.54}Se_{2.13}$ films were performed in the range of temperatures 77−400 K, frequency band $\omega = 10^2-10^6$ Hz, in zero and magnetic field of 12 kOe. The electrical resistance was measured in the temperature range 80−450 K by four-contact method.

The photoconductivities were measured by two-contact and four-contact method. The sample surface between the contacts was illuminated by laser with wavelength of 420 nm (blue color). The duration of resistance measurement under illumination was $\sim$ 1 min. The light flux power was maintained constant during the experiment.

To study the Raman spectra of polycrystalline films of $Cu_{0.27}Ga_{1.85}Se_{1.88}$ and $Cu_{0.33}Ga_{1.54}Se_{2.13}$ at room temperature a confocal spectrometer-Raman microscope SENTERRA (Bruker-Optics GmbH, Germany) with a spectral resolution $3 \div 5\,cm^{-1}$ in the measurement range $80 \div 4500\,cm^{-1}$ was used. For excitation a laser with wavelength of 523 nm (green color) was used.

3. Results and discussions

In X-ray pattern (Figure 1) of thin-film samples $Cu_{0.27}Ga_{1.85}Se_{1.88}$ (*1*) and $Cu_{0.33}Ga_{1.54}Se_{2.13}$ (*2*) obtained at selenization temperatures T_{sel} above 400°C there is a series of diffraction lines (112), (204), (116) corresponding to the structure of chalcopyrite. With increase in the selenization temperature and change in concentration of copper and gallium in sample a slight bias of main peak (112) [26] towards the lower angles 2θ is observed (Figure 1). There is also a decrease in the intensity of peak (112) associated with increase in the copper concentration, and decrease in the gallium concentration. The ionic radii for Cu^+ and Ga^{3+} are close in value and are 0.6 and 0.47 Å respectively [27]. The parameters of lattice cell for $Cu_{0.27}Ga_{1.85}Se_{1.88}$ $a = 5.593$ Å and $c = 10.918$ Å; for $Cu_{0.33}Ga_{1.54}Se_{2.13}$ $a = 5.5906$ Å and $c = 10.911$ Å; value of tetragonal compression for films $\gamma = c/a = 1.95$ were determined. At the selenization temperature of $T_{sel} < 400$°C in the X-ray pattern in addition to basic phase corresponding to $CuGaSe_2$ the additional lines were observed, this corresponds to phases Cu_2Se and $Cu_{0.25}Ga_{0.58}Se$ [25].

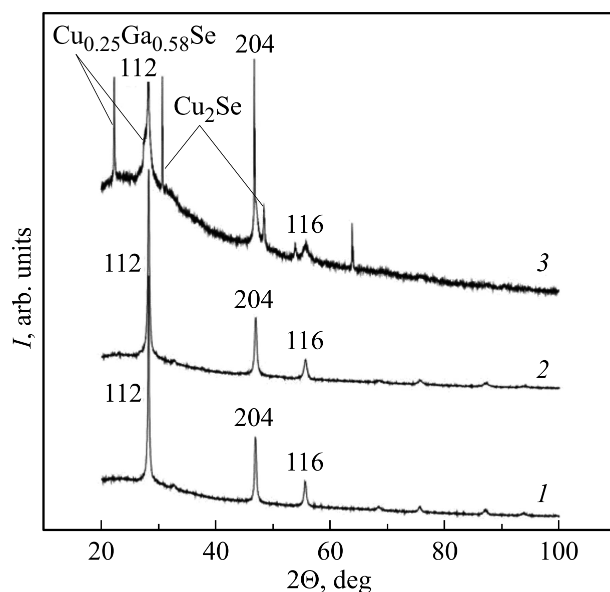

Figure 1. Data of X-ray phase analysis at $T = 25$°C of samples $Cu_{0.27}Ga_{1.85}Se_{1.88}$ (*1*) synthesized at $T = 500$°C; $Cu_{0.33}Ga_{1.54}Se_{2.13}$ (*2*) synthesized at 450°C and $CuGaSe_2$+ phase Cu_2Se + phase ($Cu_{0.25}Ga_{0.58}Se$) (*3*) [25] synthesized at $T = 350$°C.

Table 1. Semiquantitative analysis of $Cu_{0.27}Ga_{1.85}Se_{1.88}$ film

Element	norm. C [wt.%]	Atom. C [at.%]
Gallium (Ga)	43.87	46.35
selenium (Se)	50.40	47.02
Copper (Cu)	5.73	6.63
	100.00	100.00

Table 2. Semiquantitative analysis of $Cu_{0.33}Ga_{1.54}Se_{2.13}$ film

Element	norm. C [wt.%]	Atom. C [at.%]
Gallium (Ga)	36.33	38.62
selenium (Se)	56.60	53.13
Copper (Cu)	7.07	8.25
	100.00	100.00

The morphological pattern of the polycrystalline films of $Cu_{0.27}Ga_{1.85}Se_{1.88}$ (*1*) and $Cu_{0.33}Ga_{1.54}Se_{2.13}$ (*2*) with thickness about 1 μm is given in Figure 2. In the images of both film compositions the microinclusions were detected, the size of which varies within 100 nm. Tables 1, 2 present the results of a semi-quantitative analysis of the elements present (Ga, Cu, S) in samples. A decrease in the selenization temperature for film production leads to increase in the copper concentration, and decrease in the gallium concentration in the Cu−Ga−Se system.

Figure 3 shows Raman spectra measured at room temperature on two polycrystalline films of $Cu_{0.27}Ga_{1.85}Se_{1.88}$ (*1*) and $Cu_{0.33}Ga_{1.54}Se_{2.13}$ (*2*). To identify the observed modes, the data were compared with the calculated RS spectrum obtained for the initial chalcopyrite $CuGaSe_2$ (insert to Figure 3).

The electron structure for Cu−Ga−Se crystals was calculated by the density functional theory method using CASTEP package [28]. Calculations were made for atom states on Cu configuration: $3d^{10}$, $4s^1$; Ga: $3d^{10}$, $4s^2$, $4p^1$; Se: $4s^2$, $4p^4$. The structure relaxation was carried out using the quasi-Newtonian BFGS [29] scheme for minima determination of functions of many variables in the presence

Table 3. Calculated frequencies (ν_{calc}, cm^{-1}) for samples of Cu–Ga–Se system

Type	ν_{calc}	I_{calc} (rel. units)
E	64.0	28.74
E	64.0	28.74
B_2	74.7	0.1
B_1	77.7	8.8
E	97.3	76.78
E	97.3	76.78
E	164.8	20.59
E	164.8	20.59
B_1	176.7	26.1
A_1	186.3	6319.3
B_2	202.1	410.0
E	206.3	358.38
E	206.3	358.38
E	242.1	117.24
B_2	244.4	1098.1
E	245.8	14.92
E	245.8	14.92
B_1	248.0	4.6

of the first derivative. The lattice constants and atom coordinates of the samples were optimized by minimizing the total energy. The cutoff energy convergences were set at level of 700 eV. The self-consistent total energies converged within $1.0 \cdot 10^{-9}$ eV/atom. The local density approximation (LDA) functional was used for the calculation. The structure of the original $CuGaSe_2$ compound belongs to the space group $I-\bar{4}2d$ (№ 122) [30]. In Figure 3, the insert shows the calculated RS spectrum of $CuGaSe_2$. This spectrum corresponds to the experimental spectrum of $CuGaSe_2$ [31].

Oscillation representations of particle modes in center of Brillouin zone of samples Cu–Ga–Se are as follows:
$G_{KP} = 3B_2 + 6E$ (acoustic modes not considered)

$$G_{acoustic} = B_2 + E. \quad (1)$$

$G_{KP} = A_1 + 3B_1 + 3B_2 + 6E$ (acoustic modes not considered). Here A_1 — non-degenerate symmetrical irreducible representations, B_1 and B_2 — non-degenerate anti-symmetrical irreducible representations, E — doubly-degenerate representations. Calculated active modes are shown in Table 3.

In experimental spectra shown in Figure 3, for both film compositions the intense oscillation at frequency of

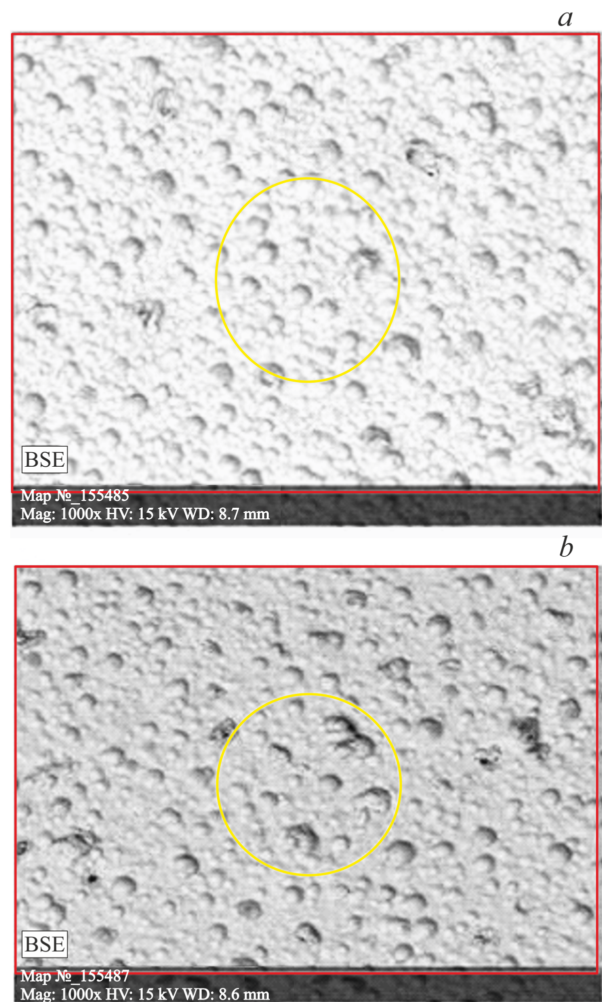

Figure 2. SEM-images of surface of $Cu_{0.27}Ga_{1.85}Se_{1.88}$ (*1*) and $Cu_{0.33}Ga_{1.54}Se_{2.13}$ films (*2*).

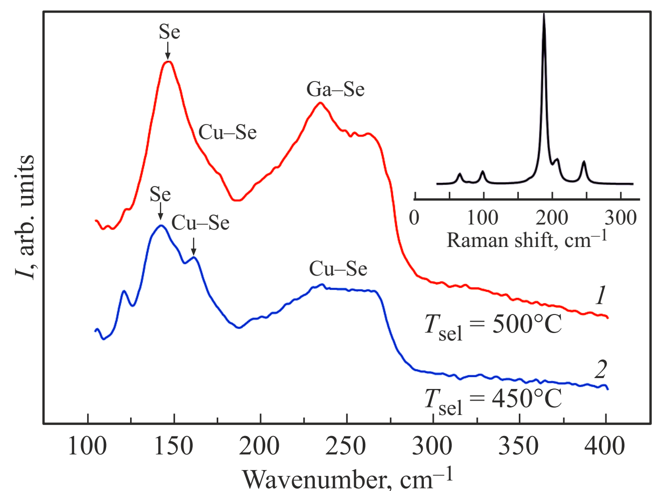

Figure 3. Raman spectra of samples $Cu_{0.27}Ga_{1.85}Se_{1.88}$ (*1*) and $Cu_{0.33}Ga_{1.54}Se_{2.13}$ (*2*) at room temperature. In insert: calculated RS spectra of $CuGaSe_2$ with chalcopyrite structure.

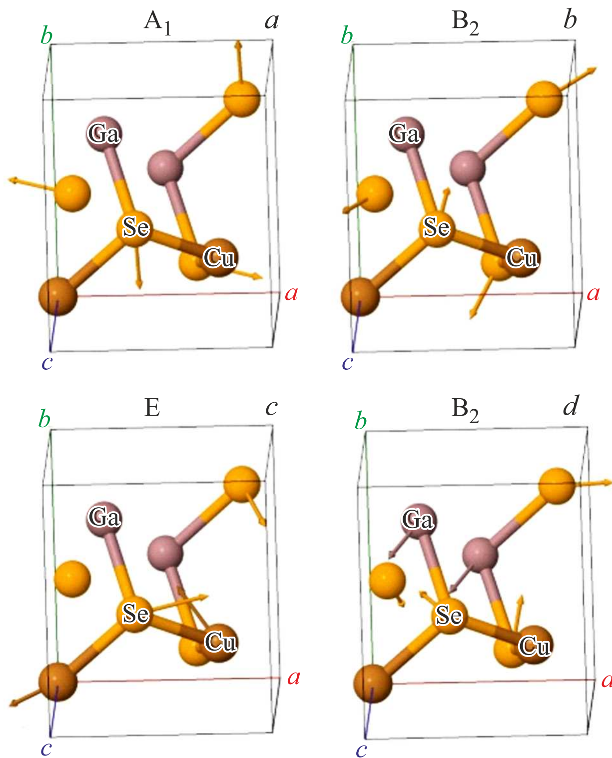

Figure 4. Simulated active oscillations of samples of Cu−Ga−Se system.

$\sim 146\,cm^{-1}$ is observed, which can be ascribed to breathing mode A_1. This mode of structural components Cu−Ga−Se occurs as result of Se atom movement, but Cu and Ga atoms remain at a standstill (Figure 4) and correspond to spectrum of $CuGaSe_2$ [31].

For $CuGaSe_2$ the oscillation frequency of spectrum is $186\,cm^{-1}$. Bias of oscillation frequency by $40\,cm^{-1}$ relative to the design frequency towards the low-frequency region, this, most likely, is associated with the presence of point defects in the sample structure The intensity of the Raman peaks presented in Figure 3 strongly depends on the surface morphology and phase composition of films synthesized at different selenization temperatures. Films with structural defects produce weak peak A_1. Double peak at frequencies 234, 260 and $122\,cm^{-1}$ refer to gallium selenides, peak at $160\,cm^{-1}$ corresponds to oscillations of components based on Cu−Se.

Figure 3 shows that in film with $Cu_{0.33}Ga_{1.54}Se_{2.13}$ composition, obtained at $T = 450°C$ the oscillation of component Cu−Se is more intense then in film with $Cu_{0.27}Ga_{1.85}Se_{1.88}$ composition (*1*), obtained at $T = 500°C$. In sample $Cu_{0.33}Ga_{1.54}Se_{2.13}$ (*2*) copper concentration is higher, hence oscillation is more intensive, at the same time the peaks corresponding to oscillations of components Ga−Se are less intensive due to decreased gallium concentration in the sample.

The transport properties of thin-film samples $Cu_{0.27}Ga_{1.85}Se_{1.88}$ (*1*) and $Cu_{0.33}Ga_{1.54}Se_{2.13}$ were studied (*2*). The synthesized samples were divided into two types, i.e. high-resistance $Cu_{0.27}Ga_{1.85}Se_{1.88}$ with activation energy $E_a = 0.3\,eV$ (Figure 5, *a*), and low-resistance $Cu_{0.33}Ga_{1.54}Se_{2.13}$ (Figure 5, *b*). May be this difference is caused by selenium deficiency, which is present in high-resistance samples compared to low-resistance samples. Decrease in copper concentration in the sample $Cu_{0.27}Ga_{1.85}Se_{1.88}$ results in the impurity subband formation, and conductivity is determined by interband transitions. The plateau observed on the dependence $\log(\rho(T))$ at $T = 320\,K$ for these samples confirms the assumptions on impurity conductivity. For samples $Cu_{0.33}Ga_{1.54}Se_{2.13}$ the dependence $\rho(T)$ has two plateaus (Figure 5, *b*) when the conductivity is maximum. The first anomaly detected at $T = 170\,K$ is most likely caused by the electron structure rearrangement of the sample. The second anomaly is observed at room temperature.

The impedance spectroscopy method was used to measure the active resistance and reactance of polycrystalline samples $Cu_{0.33}Ga_{1.54}Se_{2.13}$ in the temperature range 80−380 K, no dependence on the magnetic field was observed (Figure 6). With increase in temperature, the values of the active resistance (R) and reactance (X) increase in absolute value and their frequency dependencies change. The curves $R(\omega)$ and $X(\omega)$ were described by the Debye model, and the relaxation time was calculated, which is $\tau \sim 10^{-4}-10^{-5}\,s$ at temperatures above 300 K.

$$R(\omega) = \frac{A}{1+(\omega\tau)^2}; \quad X(\omega) = \frac{B_{\omega\tau}}{1+(\omega\tau)^2}, \qquad (2)$$

where A and B — constant parameters and are independent of temperature, τ — relaxation time of current carriers.

The localization of electrons in quantum wells determines the capacitive contribution to the linear dependence $X(\omega)$. As discussed above, the sample of film of $Cu_{0.27}Ga_{1.85}Se_{1.88}$ has high resistance, and the measuring impedance range for the sample lies outside this range.

Transmittance spectra of films of $Cu_{0.27}Ga_{1.85}Se_{1.88}$ and $Cu_{0.33}Ga_{1.54}Se_{2.13}$, measured in range 190−3300 nm, were used to determine the band gap of the film samples (Figure 7). These spectra for both high-resistance and low-resistance films are not fundamentally different due to the slight change in copper concentration in the system under study. Figure 7, *a* shows the Tauc plot, modified for the direct interband transition, for one of the films of $Cu_{0.27}Ga_{1.85}Se_{1.88}$. The spectra of the samples under study contain at least two regions with an abrupt increase in absorption. Theband gaps E_g, equal to $E_{g1} = 1.65\,eV$ and $E_{g2} = 3.71\,eV$ correspond to them. The first band gap corresponds to $CuGaSe_2$, which, according to data [32], has a direct interband transition with band gap of 1.71 eV. E_{g2} cannot be attributed to simple phases like $Cu_{2-x}Se$ or Ga_2Se_3, since the direct transition in them lies at 2.1−2.3 and 2.07 eV respectively. Thus, this transition should be attributed to the transition between the electron states of $CuGaSe_2$, lying noticeably below the top of the

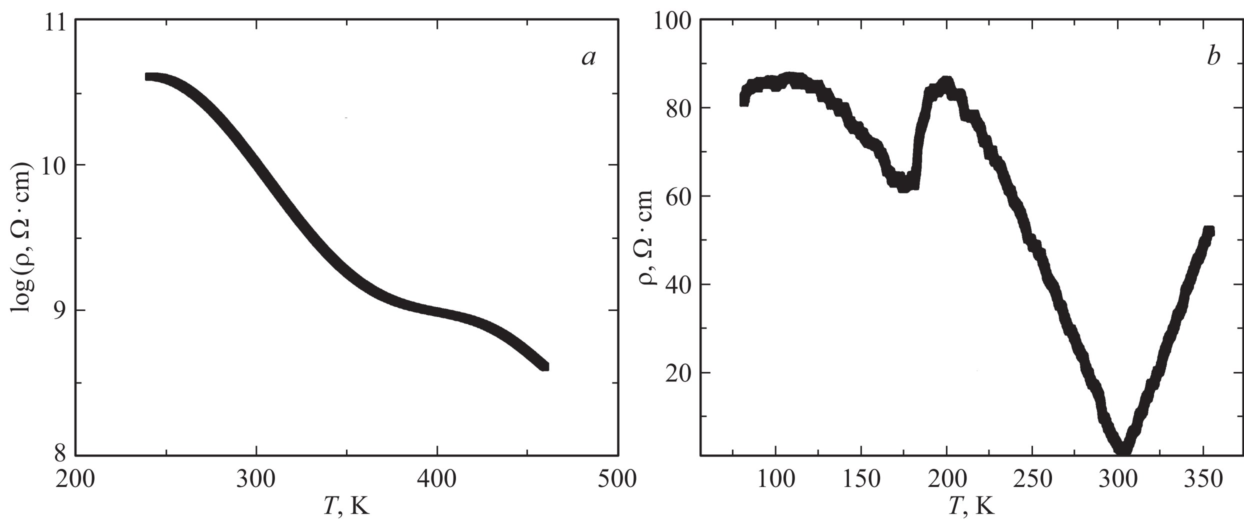

Figure 5. Resistivity of polycrystalline films of $Cu_{0.27}Ga_{1.85}Se_{1.88}$ (a) and $Cu_{0.33}Ga_{1.54}Se_{2.13}$ (b) vs. temperature.

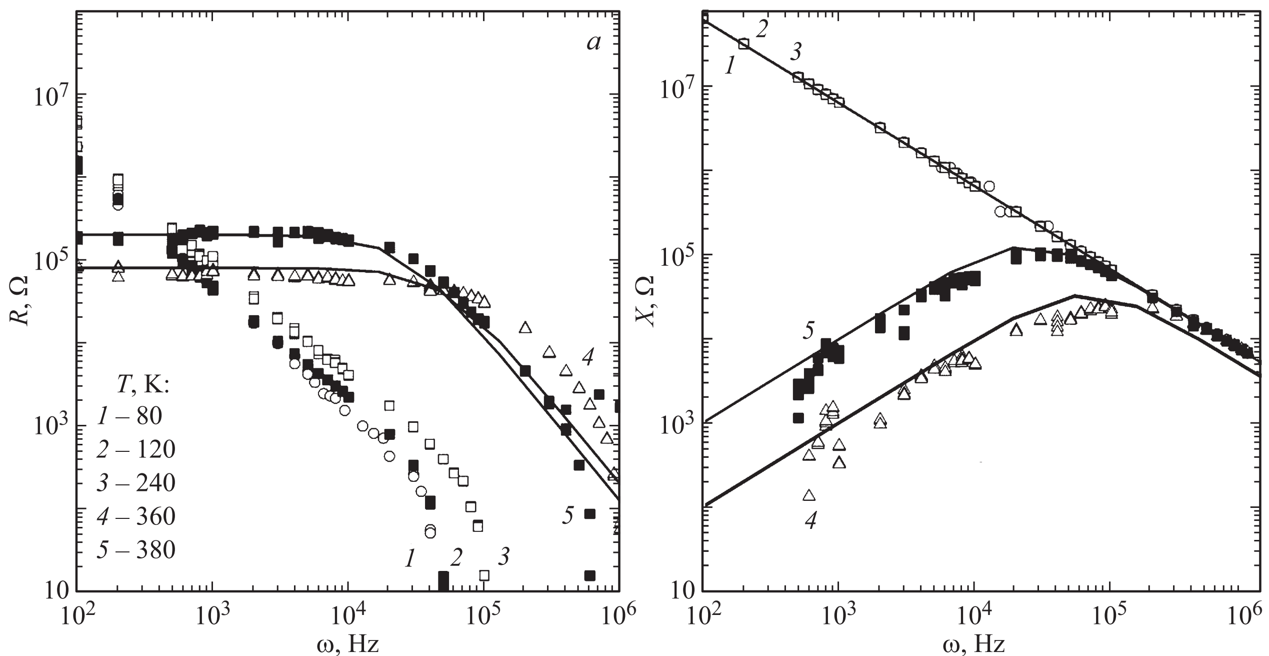

Figure 6. Active resistance (a) and reactance (b) resistances of polycrystalline films of $Cu_{0.33}Ga_{1.54}Se_{2.13}$ measured at $T = 80$, 120, 200, 240, 360, 380 K vs. frequency. Solid lines are the fitting function of the Debye model.

valence band and/or above the bottom of the conduction band. Hence, the direct gap in the spectrum of electron excitations does not affect the conductivity, which is of impurity-defect nature. From the curve of the absorption logarithm versus the photon energy (Figure 7, b), the Urbach energy was determined, which is an indicator of the scale of energy disorder at the edges of semiconductor bands. There are two linear sections on this curve (below E_{g1} and above E_{g1}), each of which has a slope ratio of $1.1\,eV^{-1}$. Hence, the Urbach energy is approximately $E_U = 0.9\,eV$, indicating large fluctuations in the energy structure. This value of the Urbach energy can be explained by change in concentration of Ga in a similar material of $Cu(In,Ga)Se_2$ [33] and of copper through the thickness of the film of $Cu_{0.27}Ga_{1.85}Se_{1.88}$, which was established during the process of selenization.

Experiments determined that only high-resistance films of $Cu_{0.27}Ga_{1.85}Se_{1.88}$ have photosensitivity (Figure 8). Under the influence of laser radiation with wavelength of 420 nm the current density increases by more than an order of magnitude during heating and reaches a maximum at $T = 320\,K$, where, according to the data of electrical properties, the electron concentration at the chemical potential level increases sharply. Since the level of chemical potential

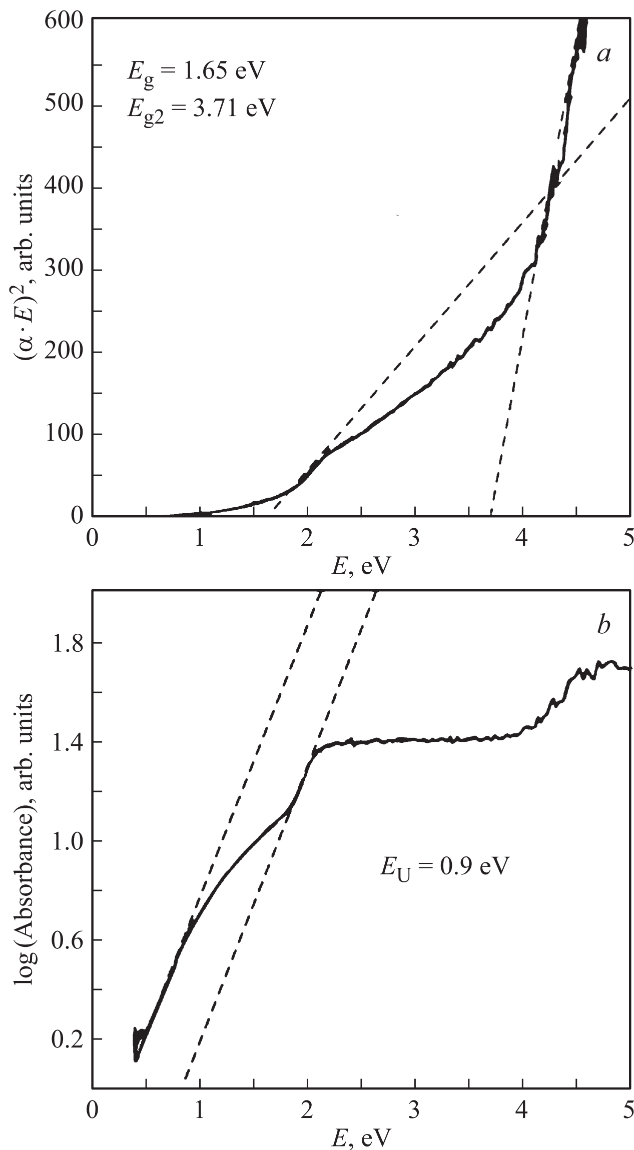

Figure 7. Tauc plot (*a*) for film of $Cu_{0.27}Ga_{1.85}Se_{1.88}$ and Urbach energy (*b*).

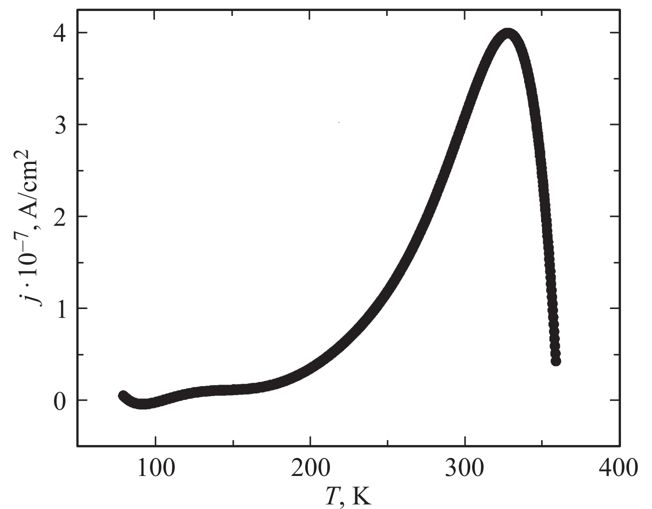

Figure 8. Current density vs. temperature during illumination of sample $Cu_{0.27}Ga_{1.85}Se_{1.88}$ laser radiation with wavelength of 420 nm.

is a function of the material, which strongly depends, in this case, on the concentration and type of carriers in the film, and therefore determines the behavior of $Cu_{0.27}Ga_{1.85}Se_{1.88}$ system. With temperature increasing the value of the current density sharply decreases. Low-resistance samples $Cu_{0.33}Ga_{1.54}Se_{2.13}$ do not exhibit the photoconductivity effect.

Figure 9 shows capacitance $C(\omega)$ vs. frequency measured in temperature range 77–400 K and frequency range $\omega = 10^2-10^6$ Hz, of film of $Cu_{0.27}Ga_{1.85}Se_{1.88}$. The measurements were carried out in zero magnetic field and in field of 8 kOe applied parallel to the capacitor plates, but no dependence on the field was found. On the curve $C(\omega)$ two frequency regions can be distinguished, low-frequency $\omega < \omega_c = 10^4$ Hz and high-frequency $\omega > \omega_c$, which are adequately described by the Debye model.

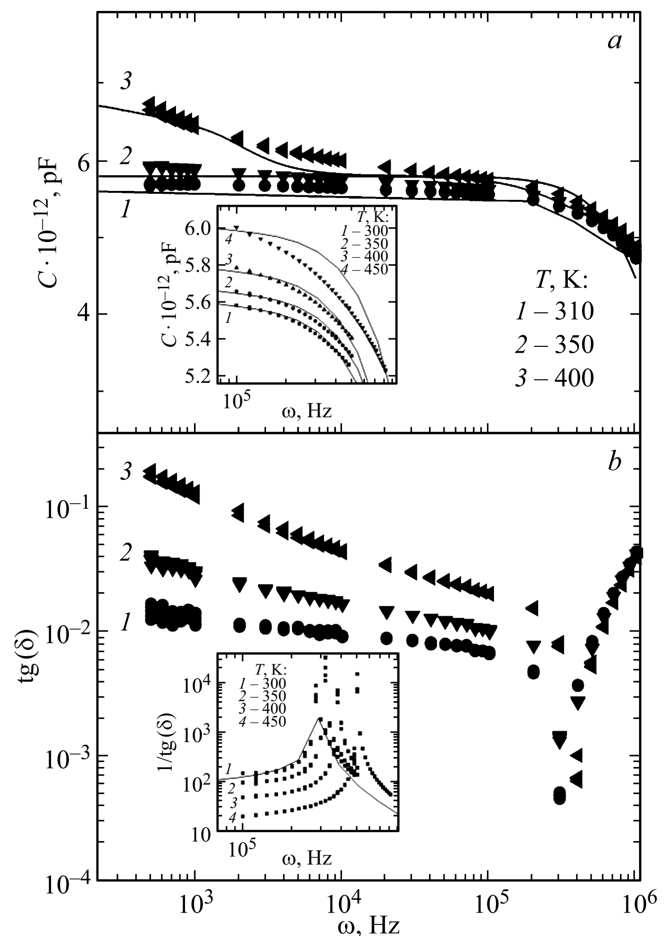

Figure 9. Capacitance (*a*) and dielectric loss tangent (*b*) vs. frequency for sample $Cu_{0.27}Ga_{1.85}Se_{1.88}$ in temperature range 77–400 K and frequency range $\omega = 10^2-10^6$ Hz. Insert to Figure 9, *a* shows capacitance vs. frequency, and insert to Figure 9, *b* contains frequency dependence $1/\mathrm{tg}(\delta)$ respectively for same sample in zoom.

The capacitance of film of $Cu_{0.27}Ga_{1.85}Se_{1.88}$ increases when heated in the low-frequency region (Figure 9, a). This behavior is typical for dielectrics and semiconductors with migration polarization [34], which have rather large relaxation times and are observed at low frequencies. In the high-frequency region the behavior of the capacitance is characteristic of the mechanism of dipole-orientation polarization, which occurs with energy losses to overcome bonding forces and internal friction. Significant changes characteristic of this mechanism were found in the dielectric loss tangent $\mathrm{tg}(\delta)$ (Figure 9, b). This value depends on active losses, as a result of increased electron scattering by local deformations and phonons. When moving from one polarization mechanism to another, the capacitance does not change with frequency change, which indicates the absence of relaxation processes, and the dielectric loss tangent tends to zero. In the insert to Figure 9, b the dielectric loss tangent vs frequency $1/\mathrm{tg}(\delta)$ is satisfactorily described by the resonance formula

$$1/\mathrm{tg}(\delta) = \frac{A\omega^n}{\sqrt{(\omega_p^2 - \omega^2)^2 + 4\beta^2\omega^2}}, \qquad (3)$$

where A — parameter independent of frequency, ω_p — resonance frequency, ω — frequency of external electric field, β — attenuation coefficient. The maximum detected at $1/\mathrm{tg}(\delta)$ (ω) shifts towards higher frequencies when heated in accordance with equation (3).

4. Conclusion

The polycrystalline films synthesized in the temperature range $200°\mathrm{C} \le T_{\mathrm{sel}} \le 550°\mathrm{C}$ and the pressure range of the vapor-gas mixture $\mathrm{Se} + \mathrm{N_2}$ during recrystallization 10^{-1} Pa had a tetragonal chalcopyrite structure. In the composition of films of Cu–Ga–Se system the copper concentration increases with decrease in T_{sel}. Depending on the selenization temperature (T_{sel}) the single-phase films with compositions of $Cu_{0.27}Ga_{1.85}Se_{1.88}$(at $T_{\mathrm{sel}} = 500$ K) and $Cu_{0.33}Ga_{1.54}Se_{2.13}$ (at $T_{\mathrm{sel}} = 450$ K) had cell parameters $a = 5.593$ Å and $c = 10.918$ Å and $a = 5.5906$ Å and $c = 10.911$ Å respectively. The Raman spectra and calculated spectra of the obtained films of Cu–Ga–Se system are consistent with each other. They consist of lines corresponding to deformation and stretching vibrations of chemical bonds between atoms of the elements Se, Cu and Ga, lines of characteristic vibrations of Cu–Se phases, as well as lines of phases with chalcopyrite structure. Resistivity vs. temperature $\rho(T)$ of high-resistance films with composition of $Cu_{0.27}Ga_{1.85}Se_{1.88}$ with activation energy of impurity subband $E_a = 0.3$ eV, have view characteristic of materials based on $CuGaSe_2$. On dependence $\rho(T)$ of low-resistance films $Cu_{0.33}Ga_{1.54}Se_{2.13}$ two anomalies were identified, at which the conductivity reaches maximum. The first anomaly at $T = 170$ K is associated with the electron structure rearrangement, the second one is observed at room temperature. Active resistance (R) and reactance (X) of films of $Cu_{0.33}Ga_{1.54}Se_{2.13}$ measured by impedance spectroscopy in temperature range 80–380 K show that they are independent of the magnetic field, and their values increase in absolute value with temperature increasing. At temperatures above 300 K the relaxation time $\tau \sim 10^{-4}$–10^{-5}s was determined from the frequency dependences of the active resistance and reactance, which are satisfactorily described by the Debye model. In the transmission spectra of the film of $Cu_{0.27}Ga_{1.85}Se_{1.88}$ two regions with abrupt increase in absorption were detected. The band gaps $E_{g1} = 1.65$ eV and $E_{g2} = 3.71$ eV correspond to them. High-resistance films of $Cu_{0.27}Ga_{1.85}Se_{1.88}$ have photosensitivity, and if exposed to laser radiation ($\lambda = 420$ nm) the current density increases by order of magnitude during heating and achieves the maximum at $T = 320$ K. From the absorption spectra Urbach energy $E_U = 0.9$ eV was determined, which indicates a nonuniform distribution of localized stated in the structure of films. The capacitance vs. frequency curve $C(\omega)$ distinguishes two frequency bands, the low-frequency $\omega < \omega_c = 10^4$ Hz and high-frequency $\omega > \omega_c$, which ensure evaluation of the migration and dipole-orientation contributions to the electrical polarization of films.

Funding

The work was carried out within the framework of the scientific topic of the State Assignment of the Institute of Physics of the Siberian Branch Russian Academy of Sciences. Study of microstructure of polycrystalline films of $Cu_{0.27}Ga_{1.85}Se_{1.88}$ and $Cu_{0.33}Ga_{1.54}Se_{2.13}$ was performed using the electron microscope of Krasnoyarsk Regional Center for Collective Use of Federal Research Center of Krasnoyarsk Scientific Center of Siberian Branch of RAS.

Conflict of interest

The authors declare that they have no conflict of interest.

References

[1] S.N. Mustafaeva, M.M. Asadov, D.T. Guseinov, I. Kasymoglu. Phys. Solid State **57**, 1095 (2015).
[2] S.N. Mustafaeva, S.M. Asadov, D.T. Guseinov, I. Kasimoglu. Semicond. **19**, 201 (2016).
[3] Xiaobo Hu, Juanjuan Xue, Jiao Tian, GuoenWeng, Shaoqiang Chen. Appl. Opt. **56**, 2330 (2017).
[4] D.W. Houck, S.V. Nandu, T.D. Siegler, B.A. Korgel. ACS Appl. Nano Mater. **2**, 4673 (2019)
[5] P. Jackson, D. Hariskos, R. Wuerz, O. Kiowski, A. Bauer, T.M. Friedlmeier, M. Powalla. pss (RRL) **9**, 28 (2015).
[6] M.A. Green, K. Emery, Y. Hishikawa, W. Warta, E.D. Dunlop. Prog. Photovoltaics **24**, 905 (2016).
[7] P. Jackson, D. Hariskos, E. Lotter, S. Paetel, R. Wuerz, R. Menner, W. Wischmann, M. Powalla. Prog. Photovoltaics **19**, 894 (2011).
[8] G.J. Bauhuis, P. Mulder, E.J. Haverkamp, J.C.C.M. Huijben, J.J. Schermer. Sol. Energy Mater. Sol. Cells **93**, 1488 (2009).

[9] Abderrahmane Belghachi, Naima Liman. Chin. J. Phys. **55**, 1127 (2017).
[10] Y. Xu, J.N. Munday. IEEE J. Photovoltaics **4**, 233 (2014).
[11] B. Mahmoudi, F. Caddeo, T. Lindenberg, T. Schneider, T. Hölscher, R. Scheer, W. Maijenburg. Electrochim. Acta **367**, 13718 (2021).
[12] I. Kasmoglu, T.G. Kerimova, I.A. Mamedova. J. Semicond. **45**, 30 (2011).
[13] O.C. Cantser, L.L. Kulyuk, T.D. Shemakova, A.V. Siminel, V.E. Tezlevan. Jpn. J. Appl. Phys. **32**, 630 (1993).
[14] S. Levchenko, N.N. Syrbu, V.E. Tezlevan, E. Arushanov, J.M. Merino, M. Leon. J. Phys. D **41**, 055403 (2008).
[15] M. Rusu, S. Doka, C.A. Kaufmann, N. Grigorieva, Th. Schedel-Niedrig, M.Ch. Lux-Steiner. Thin Solid Films **480–481**, 341 (2005).
[16] Shogo Ishizuka. Phys. Status Solidi A **216**, 1800873 (2019).
[17] V. Nadenau, U. Rau, A. Jasenek, H.W. Schock. J. Appl. Phys. **87**, 584 (2000).
[18] Shigeru Ikeda, Wakaba Fujita, Riku Okamoto, Yoshitaro Nose, Ryoji Katsube, Kenji Yoshinoand Takashi Harada. RCS Adv. **10**, 40310 (2020).
[19] M.M. Islam, T. Sakurai, A. Yamada, S. Otagiri, S. Ishizuka, K. Matsubara, S. Niki, K. Akomoto. Sol. Energy Mater Sol. Cells **95**, 231 (2011).
[20] D. Schmid, M. Ruckh, F. Grunwald, H.W. Schock. J. Appl. Phys. **73**, 2902 (1993).
[21] K. Sakurai, R. Hunger, N. Tsuchimochi, T. Baba, K. Matsubara, P. Fons, A. Yamada, T. Kojima, T. Deguchi, H. Nakanishi, S. Niki. Thin Solid Films **431–432**, 6 (2003).
[22] S. Ishizuka, J. Nishinaga, K. Beppu, T. Maeda, F. Aoyagi, T. Wada, A. Yamada, J. Chantana, T. Nishimura, T. Minemoto, M.M. Islam, T. Sakurai, N. Terada. Phys. Chem. Chem. Phys. **24**, 1262 (2022).
[23] M.M. Islam, A. Yamada, T. Sakurai, M. Kubota, S. Ishizuka, K. Matsubara, S. Niki, K. Akimoto. J. Appl. Phys. **110**, 014903 (2011).
[24] U. Rau, H.W. Schock. Appl. Phys. A **69**, 131 (1999).
[25] T.M. Gadzhiev, M.A. Aliev, A.M. Ismailov, A.M. Aliev, G.A. Aliev, Z.Kh. Kalazhokov, M.R. Tlenkopachev, Kh.Kh. Kalazhokov, A.Sh. Asvarov, A.E. Muslimov, V.M. Kanevsky. J. Surf. Invest.: X-Ray, Synchrotron Neutron Tech. **12**, 65 (2022).
[26] D.S. Su, W. Neumann, M. Giersig. Thin Solid Films **361–362**, 218 (2000).
[27] CRC Hand book of Chemistry and Physics / Ed. D.R. Lide. CRC Press (2004).
[28] S.J. Clark, C.J. Pickard, P.J. Hasnip, K. Refson, M.C. Payne, K. Refson, M. Payne. Z. Kristallogr.-Cryst. Mater. **220**, 567 (2005).
[29] B.G. Pfrommer, M. Côté, S.G. Louie, M.L. Cohen. J. Comput. Phys. **131**, 233 (1997).
[30] M. Souilah, A. Lafond, C. Guillot-Deudon, S. Harel, M. Evain. J. Solid State Chem. **183**, 2274 (2010).
[31] C. Rincon, F.J. Ramirez. J. Appl. Phys. **72**, 4321 (1992).
[32] N.A. Abdullaev, Kh.V. Aliguliyeva, L.N. Aliyeva, I. Qasimoglu, T.G. Kerimova. J. Semicond. **49**, 428 (2015).
[33] T. Klinkert, M. Jubault, F. Donsanti, D. Linco. J. Renew. Sustain. Energy. **6**, 11403 (2014).
[34] P.T. Oreshkin, B.K. Starchenkov, L.P. Andreeva. Sov. Phys. J. **13**, 556 (1970).

Translated by I.Mazurov